Scour reduction in sand beds against vertical jets by applying sheet-like countermeasures

Takegawa, Naoki

Sawada, Yutaka

Kawabata, Toshinori

Scour reduction in sand beds against vertical jets by applying sheet-like countermeasures

Naoki Takegawa[a,b], Yutaka Sawada[b,*] and Toshinori Kawabata[b]

[a] National Metrology Institute of Japan, National Institute of Advanced Industrial Science and Technology, Tsukuba, Japan

[b] Graduate School of Agricultural Science, Kobe University, Kobe, Japan

*corresponding author

Naoki TAKEGAWA

INSTITUTION 1: National Metrology Institute of Japan, National Institute of Advanced Industrial Science and Technology, Tsukuba, Japan (1-1-1, Umezono, Tsukuba, Ibaraki, 305–8563, Japan)

INSTITUTION 2: Graduate School of Agricultural Science, Kobe University, Kobe, Japan

(1-1 Rokkodai, Nada, Kobe, Hyogo, 657-8501, Japan)

Email: takegawa-naoki@aist.go.jp

Tel: +81 29 862 6359

Yutaka SAWADA (Corresponding author)

Graduate School of Agricultural Science, Kobe University, Kobe, Japan

(1-1 Rokkodai, Nada, Kobe, Hyogo, 657-8501, Japan)

Email: sawa@harbor.kobe-u.ac.jp

Tel: +81 78 803 5902

Toshinori KAWABATA

Graduate School of Agricultural Science, Kobe University, Kobe, Japan

(1-1 Rokkodai, Nada, Kobe, Hyogo, 657-8501, Japan)

Email: kawabata@kobe-u.ac.jp

Tel: +81 78 803 5800

Scour reduction in sand beds against vertical jets by applying sheet-like countermeasures

Abstract

The scour observed at the landside ground behind coastal protection facilities, such as seawalls and coastal dikes, due to tsunami overflows is the main reason for failures in such constructions. In this study, we focused on sheet-like (two-dimensional) scour countermeasures, which do not require large-scale excavation of the ground, and experimentally verified the effects of geonet and mesh sheets. By applying a vertical jet directly on the ground and increasing the external force, a situation close to the real scale conditions was reproduced. The experimental results show that the geonet material is able to significantly reduce the scour depth on both non-liquefied and liquefied grounds. We show that in the most effective case, the maximum pore-water pressure and the scour depth are reduced by about 91% and 86%, respectively, by the mesh sheet on the sand-bed surface.

Keywords: scour; vertical-jet flow; scour countermeasure; geonet; mesh sheet; upward-hydraulic gradient; hydraulic experiment.

1. Introduction

In the Great East Japan Earthquake of 2011, a huge tsunami destroyed many coastal protection facilities, such as seawalls and coastal dikes. Field surveys and model experiments have shown that the scour formed at the landside ground behind the coastal facilities as a result of the tsunami overflow is one of the main factors affecting stability (Kato et al. 2012; Kawasaki 2012; Mikami et al. 2012; Tokida and Tanimoto 2012; Tokida and Tanimoto 2014). In Japan, a massive tsunami caused by huge earthquakes is expected within the next 30 years. Furthermore, scour phenomena with overflow are caused not only by tsunamis but can also be triggered by heavy rainfalls, such as those observed in recent years; they are also the cause of failures in earth dams. Therefore, it is extremely important to understand the scour phenomenon and establish an effective

design method for scour countermeasures. The following two points are necessary to establish a scour countermeasure:

One is the expansion of options considering economics. In an island country like Japan, the total length of the coastline is huge, and it is desirable to minimize the construction costs required for the scour countermeasures. Most of the scour countermeasures that have been proposed in previous studies are based on covering the landside ground behind coastal protection facilities with heavy materials such as concrete blocks; for instance, Iiboshi et al. (2015) and Mitobe et al. (2014) demonstrated experimentally that placing concrete blocks on the ground behind a coastal dike could change the direction of the water overflow horizontally so that a scour hole was developed away from the coastal dike. In addition, Hazarika et al. (2015) and Chaudhary et al. (2018) reported that using a gabion to protect the foundation of the breakwater could almost hinder the formation of a scour. However, scour countermeasures using heavy objects involve large-scale excavation and transportation. Therefore, there is concern that the construction costs will increase.

Another point to be considered for the scour countermeasures is the liquefaction of the ground. The groundwater level is high in the vicinity of coastal structures and the ground is composed of sand particles with a uniform particle size. Therefore, there is a high possibility that liquefaction may occur as a result of an earthquake. It has been suggested that in the Great East Japan Earthquake, both a tsunami and liquefaction may have occurred at the same time (Fukumoto et al. 2012), and that liquefaction may have happened during tsunami drawdown (Sawada et al. 2014 and Tonkin et al. 2003). The authors carried out small hydraulic model experiments and found that the effect of liquefaction by upward seepage flow on the scour near the slope structures simulating a coastal dike was small (Takegawa et al., 2018). However, when heavy materials, such

as concrete blocks or gravel, are used as scour countermeasure works, there is a concern about the decrease in the bearing capacity and the settlement of the countermeasure works due to liquefaction.

In summary, it is essential to establish a new and effective countermeasure —not only for the scour but also for liquefaction— which may replace the current scour countermeasures. We proposed a method based on using sheet-like (two-dimensional) scour countermeasures that has never been proposed in previously conducted research and mentioned “Economic efficiency of the scour countermeasures” and “Robustness against liquefaction and seismic motion” as the reasons for using them (Takegawa et al., 2019). As mentioned above, although many studies on scour countermeasures have been performed so far, there is a problem where the external force is small compared to the actual phenomenon. It has not been fully verified whether the scour countermeasure works effectively when the external force increases.

In this study, instead of conducting model experiments, a situation similar to real scale conditions was locally reproduced by simplifying the overflow phenomenon and increasing the external force with a vertical jet. Research on scour using a submerged vertical water jet has been investigated in many studies (Rajaratnam 1981; Aderibigbe and Rajaratnam 1996; Yeh et al. 2009; Matsuda et al. 2014; Matsuda et al. 2016). Aderibigbe and Rajaratnam (1996) proposed the following formula for estimating the asymptotic scour depth $\varepsilon_{m\infty}$ using a vertical jet based on dimensional analysis and experimental results.

$$\frac{\varepsilon_{m\infty}}{h} = \left(1.26{E_c}^{0.11} - 1\right) \tag{1}$$

where h is the impinging distance (distance in water between the jet outlet and the initial bed surface), and E_c is the erosion parameter defined by equation (2).

$$E_c = \frac{U_0 \frac{d}{h}}{\sqrt{gD\frac{\Delta\rho}{\rho}}} \quad (2)$$

U_0 is the jet velocity, d is the jet diameter, g is the acceleration due to gravity, D is the median bed particle sizes, $\Delta\rho$ is the difference between the densities of sand and water, and ρ is the fluid density. E_c is an important parameter that determines the characteristic lengths of the scour profile. Yeh et al. (2009) modified the formula proposed by Aderibigbe and Rajaratnam (1996). As we will describe later, h and E_c cannot be used under the present experimental conditions. Apart from the experimental conditions in which a vertical jet was used, we focused on sheet-like (two-dimensional) scour countermeasures which do not require large-scale excavation of the ground and experimentally verified the effects. We examined: 1) the scour-reduction effect for each countermeasure work, 2) the effect of the above-mentioned countermeasures on the variation and increase of the pore-water-pressure, and 3) the influence of the sheet characteristics (i.e., coverage ratio and mesh size) on the scour depth and pore-water-pressure.

2. Outline of the Model Experiment

Figure 1 shows a schematic diagram of the hydraulic experiment. Using silica sand, which is generally present near the coast, to reproduce the same sand-bed conditions for all the studied cases, a sand bed with a relative density of about 30% was prepared by the water-pluviation method. The physical properties of the silica sand and the size distribution are shown in **Table 1** and **Fig. 2**. Three pore-water-pressure gauges (manufacturer: SSK, model number: P306A, capacity: 0.2 kgf/cm^2, diameter: 6 mm) were installed at the front of the acrylic wall in the sand bed. During the experiment, a vertical jet (flow rate: 190 L/min, flow velocity U_0: 4.2 m/s, jet diameter d: 0.031 m) simulating the overflow water caused by the tsunami was applied to the sand bed for 1 min, and the scour progress was recorded as images using a video camera. The scour depth and scour diameter shown in **Fig. 3** were calculated by counting the number of pixels in the obtained images. To prevent an increase in the water level due to the vertical jet in the acrylic water tank, water was drained at the height near the initial bed surface. The momentum flux ($=\rho Qv$) of the vertical jet in this experiment was larger than those reported in the studies conducted by Rajaratnam (1981), Aderibigbe and Rajaratnam (1996), Matsuda et al. (2014), and Matsuda et al. (2016). Additionally, in the previous studies, scour on the seabed or the riverbed, that is, scour in water, was assumed, and the area between the jet outlet and the initial bed surface was filled with water (impinging distance h). On the other hand, in this study, we assume that the landside ground is scoured by the tsunami, which overflows the coastal protection facilities. The vertical jet directly acts on the sand bed, and no water exists between them. Therefore, E_c derived from h cannot be defined, which is a characteristic that distinguishes it from previous studies. **Figure 3** shows the difference between the experimental conditions in the previous and present studies.

To verify whether the scour countermeasures had a noticeable effect even during liquefaction, the upward seepage flow was given by the head difference in the same manner as in previous studies (Takegawa et al., 2018), and the effective stress in the sand bed was controlled. The upward-hydraulic gradient i (=H/L) was determined as i = 1.0 from the relationship between the head difference and the excess-pore-water-pressure ratio (EPWPR, $\Delta u/\sigma_0'$) obtained from the previous experiment. EPWPR is a dimensionless number expressed as the ratio of the initial effective stress σ_0' to excess-pore-water pressure Δu generated by the upward-hydraulic gradient. The excess-pore-water pressure Δu is calculated from the water depth and the water pressure measured by the gauges shown in **Fig. 1 (a)**. When i = 1.0, EPWPR is about 0.75 in this experiment, which is the maximum value obtained where boiling does not occur with the progress of the scour. The ground where no upward-hydraulic gradient is acting is called "standard bed" and the ground where an upward-hydraulic gradient is acting is called "low bearing capacity bed (LBC-bed)" for distinction.

Table 2 shows the experimental cases: In Cases 3–11, geonet, gravel, and mesh sheets were adopted as scour countermeasures (**Fig. 4**). The geonet material used in Cases 3 and 4 is mainly made of polyethylene and is fixed on the initial bed surface so that it is not moved by the vertical jet during the experiment. The gravel used in Cases 5 and 6 had a median particle diameter D_{50} of about 15 mm, and the backfill thickness was 10 cm. In Cases 2, 4, and 6, an upward-hydraulic gradient was applied to the sand bed to reproduce low effective stress conditions. The mesh sheets made of stainless steel used in Cases 7–11 had different mesh sizes and coverages. Here, the coverage ratio is the proportion of scour countermeasures per unit area. The installation situation is the same as in the case of using geonet. We examined the influence of the sheet

characteristics on the scour-reduction effect by changing the coverage ratio in Cases 7–9 and changing the mesh size in Cases 9–11.

3. Experimental Result

3.1 Scour-reduction effect for each scour countermeasure (Cases 1–6)

Figure 5 shows the scour process on standard beds for Cases 1, 3, and 5, while **Fig. 6** shows the time variations of the scour depth on both standard and LBC-beds for Cases 1–6.

For the standard bed, in Case 1 (no countermeasure), the scour depth increases rapidly after the vertical-jet flow acts on the sand bed and reaches a constant value after 30 s from the start of the experiment. The scour depth at the end of the experiment is about 52 cm. From the image obtained during the experiment, the maximum rise in water level by the vertical jet was observed to be about 5 cm (0.5 kPa). Using the increased water depth as the impinging distance h defined in previous studies, the present experimental result of the maximum scour depth for Case 1 is compared with the prediction formulas proposed by Aderibigbe and Rajaratnam (1996) and Yeh et al. (2009). The comparisons are listed in **Table 3**. Note that h/d in this experiment is about 1.6, which does not exactly meet the applicable range proposed by Aderibigbe and Rajaratnam (1996) and Yeh et al. (2009). Basis the comparison, the maximum scour depth observed in this experiment was considerably larger than the values based on the prediction formulas. Regarding the scour at the landward ground of the coastal dike where the vertical jet is expected to directly act on the ground, h/d becomes extremely small. Therefore, the prediction formula for the scour profiles proposed in previous studies is likely to be inapplicable.

The scour depth at the end of the experiment for Case 3 (geonet, standard bed) is about 32 cm, which is about 38% below that for Case 1. The scour-reduction effect by the geonet is confirmed, even if the external force is increased, which suggests that geonet may be a simple and economical scour countermeasure. As described in detail in

Section 3.3, in Case 11, the scour depth is reduced by 86%; this is a remarkable experimental result. In Case 5 (gravel, standard bed), the gravel is eroded by the vertical jet (**Fig. 5 (b)**). As a result, the vertical jet reaches the sand bed surface and the scour depth increases. Five seconds after the start of the experiment, the scour depth is reduced in the order: geonet, gravel, and no countermeasure. However, after 5 s, the scour depth decreases by redeposition of the gravel in the scour hole and formation of a thick gravel layer (**Figs. 5 (c)–(e)**). Although it is difficult to verify whether or not redeposition of the gravel occurs in the actual site, there is a possibility in the present experiments that the scour depth may be underestimated while it decreases (Case 5: 5-10 s, Case 6: 10-20 s). Therefore, in cases using gravel, the results after the redeposition are not discussed.

For the LBC (low bearing capacity) bed, the scour depths obtained in Cases 2 (no countermeasures, LBC-bed) and 4 (geonet, LBC-bed) are below the value measured for the standard bed after 1 s from the start of the experiment. This result indicates that the scour depth does not increase even though the effective stress in the sand bed decreases. This is because —as described previously (Takegawa et al., 2018)— the scour phenomenon depends on the relationship between the resistance of the sand particles on the bed surface and the tractive force acting on them, and the excess-pore-water pressure is completely dissipated on the bed surface. Therefore, the effect of the upward-hydraulic gradient on the sand particles is small as long as no boiling occurs. In addition, the reason the scour depth for LBC-bed is below that observed for the standard bed is possibly because of a decrease of the effective stress in the sand bed. When focusing on the sand mass at the slope where the upward-hydraulic gradient is applied, the sliding moment of the sand mass is constant, while the resistance moment decreases with an increase of excess-pore-water pressure. It means that slope failures are more

likely to occur because if the upward-hydraulic gradient compared with the standard bed. Therefore, as a result of frequent slope failures, a large amount of sand particles deposits at the bottom of the scour hole, and the scour depth decreases. **Figure 7** shows the time variation of the scour diameter. After 10 s from the start of the experiment, the scour diameter in the LBC-bed is larger than that for the standard bed in each experimental case. It is understood that in LBC-bed, the scour diameter increases due to the slope failure. Although a decrease in the scour depth was observed in the LBC-bed for Cases 2 and 4, it should be noted that the deterioration of the coastal dikes themselves due to liquefaction needs to be evaluated separately from the scour phenomenon.

Unlike the results obtained in Cases 2 (no countermeasures, LBC-bed) and 4 (geonet, LBC-bed), the scour depth for Case 6 (gravel, LBC-bed) is larger than that observed for the standard bed at all times. The maximum scour depths for Cases 5 (gravel, standard bed) and 6 are 24 cm (t=5 s) and 38 cm (t=10 s), respectively. In particular, the maximum scour depth reported for Case 6 is the largest value obtained for all the cases with countermeasures. This is because the effective stress in the sand bed decreases due to upward seepage (upward-hydraulic gradient) and the bearing capacity against the gravel also decreases. **Figure 8** shows the scour profiles for Cases 5 and 6 at 5 s. These results show that when heavy materials, such as gravel and concrete block, are used as the scour countermeasure, it is necessary to prevent the settlement of the countermeasure work. It is also important to verify whether the scour-reduction effect occurs or not, even during liquefaction.

3.2 Variation of the pore-water pressure for each scour countermeasure (Cases 1, 3, and 5)

Figure 9 shows the increase in the pore-water pressure during the experiment. **Figs. 9 (a)–(c)** correspond to the values of the pore-water-pressure gauges 1, 2, and 3. Each pore-water-pressure gauge is placed at the position shown in **Fig. 1 (a)**. The vertical line shown in **Figure 9** is the time when the gauge was exposed to water as the scour progressed.

In **Fig. 9 (a)**, The value of the pore-water-pressure gauge 1 increases rapidly when the vertical jet acts on the sand bed. It can be seen that the value reaches about 3.4 kPa for Case 1 (no countermeasure, standard bed), about 3.2 kPa for Case 5 (gravel, standard bed), and about 1.6 kPa for Case 3 (geonet, standard bed). This rapid pressure increase is caused by the vertical jet colliding with the initial bed surface, and the vertical momentum is converted to pressure. Although the pressure generated by the collision of the vertical jet depends on the deformation process of the fluid and the sand bed, as a reference, it is noted that the stagnation pressure of the vertical jet is about 8.8 kPa. The local pressure generated by the vertical jet is dispersed inside the sand bed. Therefore, the maximum value of the pressure in each case is lower than the stagnation pressure. In particular, in Case 3, the increment of the pore-water pressure is suppressed to about half compared to Cases 1 and 5. The effect of dispersing and reducing the collision force by the geonet against the force transmitted to the ground with the falling rock has been confirmed in previous studies related to the field of civil engineering. The coverage ratio of the geonet used in this experiment is about 52%, and it is considered that a part of the collision force of the vertical jet is borne by the tension of the geonet (hammock effect).

The pore-water pressure, which is increased by the collision of the vertical jet, decreases with the progress of time and becomes stable after 15 s from the start of the

experiment in each case. In Cases 3 and 5, the pore-water pressure after stabilization is about 1 kPa, while it vibrates at about 0 kPa in Case 1. This is because in Case 1, no sand bed is formed in the vicinity of gauge 1 with the progress of the scour, and the flow velocity of the vertical jet is hardly reduced. Conversely, in Cases 3 and 5, since the flow velocity of the vertical jet is reduced by the sand bed in the vicinity of gauge 1, the pore-water pressure after stabilization is larger than that observed in Case 1. Therefore, the pore-water-pressure in an asymptotic state is a complex phenomenon that changes significantly depending on the surrounding bed conditions. In this study, we focus on the variation of pore-water pressure that occurs at the early stages of the experiment.

The maximum values of the pore-water pressure are shown in **Figs. 9 (b)** and **9 (c)**, where they appear in the order: Case 1>Case 5>Case 3. It is also reconfirmed that the geonet suppresses the increase in the pore-water pressure in the sand bed. In **Fig. 9 (b)**, the pore-water-pressure gauge 2 is exposed to water only in Case 1, and it is clear that the fluctuation of the pore-water pressure is large after exposure. In **Fig. 9 (c)**, since the pore-water-pressure gauge 3 is located 10 cm away (horizontally) from the collision point of the vertical jet, the influence of the increase in the water level during the experiment can be clearly considered. As mentioned in section 3.1 the maximum rise in water level by the vertical jet was about 5 cm (0.5 kPa) at the point where gauge 3 was placed. Therefore, the value obtained by subtracting the effect of the water-level rise (0.5 kPa) from the increment in the pore-water pressure shown in **Fig. 9 (c)** is the net excess-pore-water pressure caused by the vertical jet. The maximum values of the net excess-pore-water pressure for Cases 1, 3, and 5 are 1.89, 0.94, and 1.74 kPa, respectively, and it can be understood that the vertical jet is de-energized by the geonet also in the evaluation based on these maximum values. The control of the increase in

pore-water pressure can be related to the relaxation of the collision force by the vertical jet, which is extremely important from the viewpoint of scour prevention. In the next section, the relationship between pore-water pressure and scour depth is discussed.

3.3 Influence of the sheet characteristics (mesh size and coverage ratio) on the scour-reduction effect (Cases 1 and 7–11)

Figure 10 shows the variation of the scour depth for the Case using mesh sheets. In Cases 7–9, the mesh size is approximately 1 mm and the coverage ratios are approximately 29% (Case 7), 42% (Case 8), and 59% (Case 9). Although the scour depths at the end of the experiment for Cases 7–9 decrease by about 19–27% compared to Case 1 (no countermeasure, standard bed), the increase in the coverage ratio does not dramatically reduce the scour depth. If the coverage ratio is 100%, although an improvement in the scour-reduction effect can be expected, it is necessary to consider the dissipation of pore-water pressure and the displacement of the countermeasure works due to uplift pressure. In addition, considering the coverage of the commonly used geonet, a verification of the coverage up to 60% is reasonable.

In Cases 9–11, the coverage ratio remains almost constant, at about 58%, and the mesh sizes are 1.02, 0.33, and 0.11 mm, respectively. At the end of the experiment, the reduction rate of the scour depth is significantly increased to 78% and 86% for Cases 10 and 11, compared to 27% for Case 9. Therefore, it is inferred that there is a threshold value for the mesh size that can significantly reduce the scour. Sherard and Dunnigan (1989) proposed a filter law for preventing runoff of soil particles from the core zone at fill dams. When this filter law is applied to the present experimental condition, the ratio ($=d_{15}/D_{85}$) between 15% particle diameter, d_{15}, of the filter material and 85% particle diameter, D_{85}, of the ground material must be smaller than 4.0. Assuming that D_{85} of the bed material is 85% particle size of the silica sand (=0.36 mm)

and d_{15} of the filter material is the mesh size m, the ratios m/D_{85} in Cases 9–11 are 2.83, 0.92, and 0.31, respectively, which are below the threshold value of the filter law of 4.0. However, in Case 9, the corresponding scour-reduction effect is not evident. Of course, it should be noted that since the geonet material is so thin, the filter law cannot be simply applied. The d_{15}/D_{85} ratio of 2.83 obtained in this experiment indicates that almost all the sand particles can pass through the mesh sheet. The experimental results thus suggest that the sand particles can easily pass through the mesh sheet when a large fluid force, such as a vertical jet, acts and the ratio is about 2.83. In Cases 10 and 11, since the scour depth is significantly reduced, the ratio between the 85% particle size of the bed material and the mesh size should be less than 1.0.

Figure 11 shows the increase in pore-water pressure from the start of the experiment measured at the pore-water-pressure gauge 1. Focusing on the coverage ratio (Cases 7–9, **Fig. 11 (b)**), the reduction rates of the maximum pore-water pressures for Cases 7 and 8 are small, and when the coverage ratio increases to 59%, the maximum pore-water pressure decreases by about 47%. Focusing on the mesh size (Cases 9–11, **Fig. 11 (c)**), the maximum pore-water pressures for Cases 10 and 11 are significantly suppressed compared to Case 9. The relationship between the maximum pore-water pressure and the mesh-sheet characteristics (i.e., coverage ratio and mesh size) is similar to that observed for the scour depth.

Figure 12 shows the effects of the coverage ratio and mesh size on the maximum pore-water pressure and the scour depth. In the vertical axis, the maximum pore-water pressures observed during the experiments and the scour depths at the end of the experiments are represented in dimensionless form for each case using the value for Case 1. The increase in coverage ratio observed in **Fig. 12 (a)** indicates that the proportion of the collision force applied to the geonet increases, which is directly linked

to the decrease in the collision force acting on the sand bed, that is, the pore-water pressure. On the other hand, because the correlation between coverage ratio and scour depth is weak, it is possible that the reduction effect of the flow velocity passing through the mesh is small even if the coverage ratio increases. In **Fig. 12 (b)**, the graphs for the maximum pore-water pressure and the scour depth are almost the same. The mesh sheet (with a small mesh size) suppresses the scour of the bed in the upper part of the pore-water pressure gauge 1. Therefore, the collision force is dispersed by the upper bed and the increase in pore-water pressure is also suppressed.

It is worth noting that in the most effective case, the maximum pore-water pressure and the scour depth were reduced by about 91% and 86%, respectively, by the mesh sheet on the sand-bed surface. In addition, knowledge about the coverage ratio and the mesh size for improving the effect of the mesh sheet is extremely important in establishing design guidelines for economical scour countermeasures.

4. Summary

In this study, we focused on sheet-like (two-dimensional) scour countermeasures that do not require large-scale excavation of the ground and experimentally verified their effects. In addition, by simplifying the overflow phenomenon and increasing the external force with a vertical jet, a situation close to the real one was reproduced. We examined: 1) the scour-reduction effect for each countermeasure work, 2) the effect of the above-mentioned countermeasures on the variation and increase of the pore-water pressure, and 3) the influence of the sheet characteristics (i.e., coverage ratio and mesh size). The obtained results are listed below:

(1) In the case of the standard bed (without upward-hydraulic gradient), the scour depth was about 52 cm at the end of the experiment without countermeasures and about 32 cm when geonet was used. This represents a reduction of about 38% compared

to the case without countermeasures. The scour-reduction effect by the geonet could be confirmed even when the external force was increased, and it is suggested that geonet may be a simple and economical countermeasure against scour.

As for the LBC bed, in the case without countermeasures and using geonet, no increase in the scour depth was observed. This is considered to be because the excess-pore-water pressure completely dissipates on the sand-bed surface, and the reduction of effective stress has little effect on the sand particles on the surface. Conversely, when gravel was used, the maximum scour depth increased by a factor of about 1.6 compared to the standard bed. This is because the effective stress decreases due to the upward-hydraulic gradient and the bearing force of the sand bed against the gravel also decreases. These results indicate that when heavy materials, such as gravel and concrete block, are used as scour countermeasures, it is necessary to prevent the settlement of the countermeasure work. It is also important to verify whether the scour-reduction effect occurs or not, even during liquefaction.

(2) The pore-water pressure increases rapidly when the vertical jet acts on the sand bed. The coverage ratio of the geonet used in this experiment was about 52%, and the collision force of the vertical jet and increase in the pore-water pressure were reduced by the tension of the geonet. In particular, the net pore-water-pressure increment (deducting the influence of the water-level rise by the vertical jet) was reduced by about 50% compared to the case without countermeasures.

(3) When the coverage ratio of the mesh sheet is kept constant and the ratios ($=m/D_{85}$) between the 85% particle size of the silica sand (=0.36 mm) and the mesh size of the mesh sheet (i.e., 1.02, 0.33, and 0.11 mm) are changed to 2.83, 0.92, and 0.31, respectively, both the scour depth and the maximum pore-water pressure are

significantly suppressed in the cases of the ratios of 0.92 and 0.31. It is understood that sand particles easily pass through the mesh sheet when a large fluid force such as a vertical jet acts and the ratio m/D_{85} is about 2.83. It is desirable to keep the ratio between the 85% particle size of the bed material and the mesh size below 1.0. In addition, although both the maximum pore-water pressure and the scour depth decrease as the coverage ratio increases, the reduction rate of the scour depth tends to be smaller. Therefore, when the ultimate goal is to reduce the scour depth, one of the most important considerations is to use a sheet-like countermeasure with a small mesh size. It is worth noting that the maximum pore-water pressure and the scour depth were reduced by about 91% and 86%, respectively, by the mesh sheet on the sand-bed surface.

Acknowledgement

The authors are grateful to Mitsui Chemicals Industrial Products Ltd. for providing the geonet.

Funding

The work reported here was supported by JSPS Grant-in-Aid for Challenging Research Exploratory No. 18K19248.

References

(1) Aderibigbe, O.O., and N. Rajaratnam. 1996. Erosion of loose beds by submerged circular impinging vertical turbulent jets. *Journal of Hydraulic Research* 34(1): 19–33.

(2) Chaudhary, B., H. Hazarika, A. Murakami, and K. Fujisawa. 2018. Geosynthetic-

sheet pile reinforced foundation for mitigation of earthquake and tsunami induced damage of breakwater. *Geotextiles and Geomembranes* 46(5): 597–610.

(3) Fukumoto, Y., H. Sukegawa, N. Iwamae, and T. Ikeya. 2012. The 2011 off the Pacific coast of Tohoku Earthquake tsunami hydraulic data observed at Choshi offshore. *Journal of Japan Society of Civil Engineers Ser.B2* 69(2):1–5. (in Japanese)

(4) Hazarika, H., K. Nishimura, and B. Chaudhary. 2015. Model testing on resilient solution for breakwater protection against tsunami. *Japanese Geotechnical Society Special Publication* 3(2): 40–44.

(5) Iiboshi, T., S. Maeno, K. Yosida, D. Takata, and A. Yamamura. 2015. Effects of landward slope protection and toe protection work shape at coastal dikes on landward bed scouring caused by tsunami overflow. *Proceeding of 36th International IAHR World Congress*, Hague, Netherlands.

(6) Kato, F., Y. Suwa , K. Watanabe, and S. Hatogai. 2012. Mechanisms of coastal dike failure induced by the Great East Japan Earthquake tsunami. *Proceeding of 33rd International Conference on Coastal Engineering*, Santander, Spain.

(7) Kawasaki, K. 2012. Fundamental characteristics of tsunami and tsunami disaster due to the 2011 off the Pacific Coast of Tohoku Earthquake. *The Japanese Society for Multiphase Flow* 26(1): 11–18. (in Japanese)

(8) Matsuda, T., K. Maeda, M. Miyake, J. Miyamoto, H. Sumida, and K. Tsurugasaki. 2014. Experimental speculation on scour due to jet flow focusing on the soil particle and the soil element scale level. *Journal of Japan Society of Civil Engineers Ser.B2* 70(2): l_1041-l_1045. (in Japanese)

(9) Matsuda, T., A. Yamaguchi, K. Maeda, K. Takagi, K. Tsurugasaki, and J. Miyamoto. 2016. Experimental study on scouring the two-layer ground due to jet flow. *Journal of Japan Society of Civil Engineers Ser.B2* 72(2): l_1195-l_1200. (in Japanese)

(10) Mikami, T, T. Shibayama, and M. Esteban. 2012. Field Survey of the 2011 Tohoku Earthquake and Tsunami in Miyagi and Fukushima Prefectures. Coastal Engineering Journal 54(1): 1250011-1–1250011-26. doi:10.1142/S0578563412500118.

(11) Mitobe, Y., M.B. Adityawan, H. Tanaka, T. Kawahara, T. Kurosawa, and K. Otsushi. 2014. Experiments on local scour behind coastal dikes induced by tsunami overflow. *Proceedings of the 34th International Conference on Coastal Engineering*, Seoul, Korea.

(12) Rajaratnam, N. 1981. Erosion by plane turbulent jets. *Journal of Hydraulic Research* 19(4): 339–358.

(13) Sawada, Y., M. Miyake, H. Sumida, and T. Kawabata. 2014. Pore water pressure and liquefaction in saturated sand bed induced by tsunami. *Irrigation, Drainage and Rural Engineering Journal* 82 (2): 113–120.

(14) Sherard, L., and P. Dunnigan. 1989. Critical filters for impervious soils. *Journal of Geotechnical Engineering* 115(7): 927–947.

(15) Takegawa, N., Y. Sawada, K. Murai, and T. Kawabata. 2018. Influence of Liquefaction on Scour behind Coastal Dikes Due to Tsunami Overflow. International Journal of Geotechnical Engineering 12 (1): 40–45. doi:10.1080/19386362.2016.1246216.

(16) Takegawa, N., Y. Sawada, and T. Kawabata. 2020. Geogrid-Based Countermeasures against Scour behind Coastal Dikes under Tsunami Overflow. Marine Georesources & Geotechnology 38 (1): 64–72. doi:10.1080/1064119X.2018.1552998.

(17) Tokida, K., and R. Tanimoto. 2012. Lessons and views on hardware countermeasures with earth banks against tsunami estimated in 2011 Great East Japan Earthquake. *Proceedings of the One Year after 2011 Great East Japan*

Earthquake International Symposium on Engineering Lessons Learned from the Giant Earthquake 9: 1–12.

(18) Tokida, K., and R. Tanimoto. 2014. Lessons for countermeasures using earth structures against tsunami obtained in the 2011 Off the Pacific Coast of Tohoku Earthquake. *Soils and Foundations* 54(4): 523–543.

(19) Tonkin, S., H. Yeh, F. Kato, and S. Sato. 2003. Tsunami scour around a cylinder. *Journal of Fluid Mechanics* 496: 165–192.

(20) Yeh, P. H., K. A., Chang, J., Henriksen, B., Edge, P., Chang, A., Silver, and A. Vargas. 2009. Large-scale laboratory experiment on erosion of sand beds by moving circular vertical jets. *Ocean Engineering* 36(3–4): 248–255.

Table Captions

Table 1 Properties of silica sand.

Table 2 Experimental conditions.

Figure Captions

Fig. 1 Experimental apparatus.

(a) Front view.

(b) Top view.

Fig. 2 Size distribution of silica sand.

Fig. 3 Difference between the experimental conditions in the previous study and the present study. (Left: Present study, Right: Previous studies conducted by Rajaratnam 1981, Aderibigbe and Rajaratnam 1996, Yeh et al. 2009, Matsuda et al. 2014, and Matsuda et al. 2016).

Fig. 4 Countermeasure work against scour used in the present experiments.

(a) Geonet (main raw material: polyethylene, mesh shape: circle, mesh size: 2.5 mm, and coverage ratio: 52.4%).

(b) Gravel (D_{50}: 15 mm).

(c) Mesh sheet for Case 7 (main raw material: stainless steel, mesh shape: square, mesh size: 1.02 mm, and coverage ratio: 29.0%).

Fig. 5 Scour profiles at 1, 10, and 30 s and at 1 min. The sand bed surfaces for Case 1 and Case 3 are represented by a solid black line. The red dashed lines indicate the installation height of the pore-water pressure gauges.

Fig. 6 Time variation of the scour depth for Cases 1–6.

Fig. 7 Time variation of the scour diameter for Cases 1–6.

Fig. 8 Scour profile at 5 s with a scour countermeasure using gravel at each hydraulic gradient.

Fig. 9 Time variation of pore-water-pressure.

(a) Pore-water pressure gauge 1.

(b) Pore-water pressure gauge 2.

(c) Pore-water pressure gauge 3 (the painted area shows the increase in water pressure due to the water-level rise).

Fig. 10 Time variation of the scour depth for Cases 1 and 7–11.

Fig. 11 Time variation of the pore-water pressure for Cases 1 and 7–11.

(a) Case 1.

(b) Cases 7–9 (Mesh size: constant).

(c) Cases 9–11 (Coverage ratio: constant).

Fig. 12 Effect of coverage ratio and mesh size on the scour depth and pore-water pressure (the value measured at the pore-water-pressure gauge 1 is used).

(a) Effect of the coverage ratio.

(b) Effect of the mesh size.

Table 1 Properties of silica sand.

Density of sand particle ρ_s (g/cm^3)	2.63
Maximum dry density ρ_{max} (g/cm^3)	1.64
Minimum dry density ρ_{min} (g/cm^3)	1.30
Median particle diameter D_{50} (mm)	0.26
Geometric standard deviation σ_g	1.38

Table 2 Experimental conditions.

ID	Countermeasure	Mesh size	Coverage ratio	Hydraulic gradient (EPWPR)
Case 1	N/A			0.0 (0.0)
Case 2				1.0 (0.75)
Case 3	Geonet	2.50 mm	52.4%	0.0 (0.0)
Case 4				1.0 (0.75)
Case 5	Gravel	N/A		0.0 (0.0)
Case 6				1.0 (0.75)
Case 7	Mesh sheet	1.07 mm	29.0%	0.0 (0.0)
Case 8		1.07 mm	42.4%	
Case 9		1.02 mm	58.8 %	
Case 10		0.33 mm	58.1%	
Case 11		0.11 mm	58.4%	

Table 3 Maximum scour depth in the present study and the calculated values using the prediction formulas proposed by Aderibigbe and Rajaratnam (1996) and Yeh et al. (2009).

	Maximum scour depth	Asymptotic scour depth $\varepsilon_{m\infty}$
Present study (h:50 mm, h/d:1.6)	520 mm	
Aderibigbe and Rajaratnam (1996) Applicability range (h/d > 8.3)		45 mm
Yeh et al. (2009) Applicability range (h/d is around 6)		29 mm

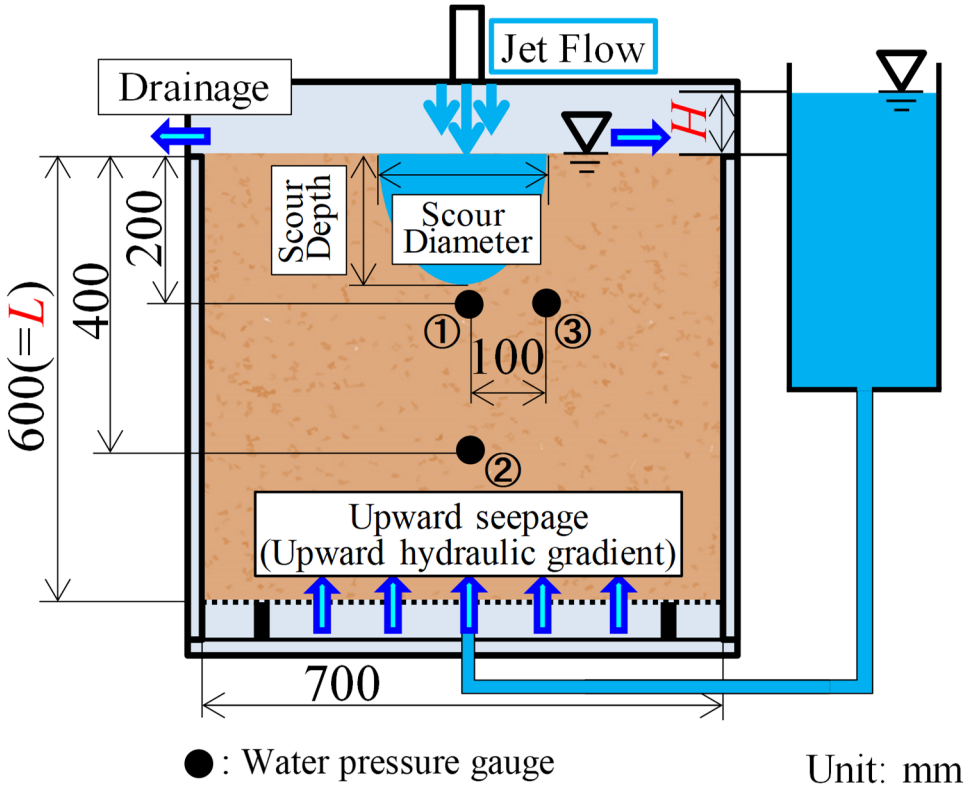

(a) Front view.

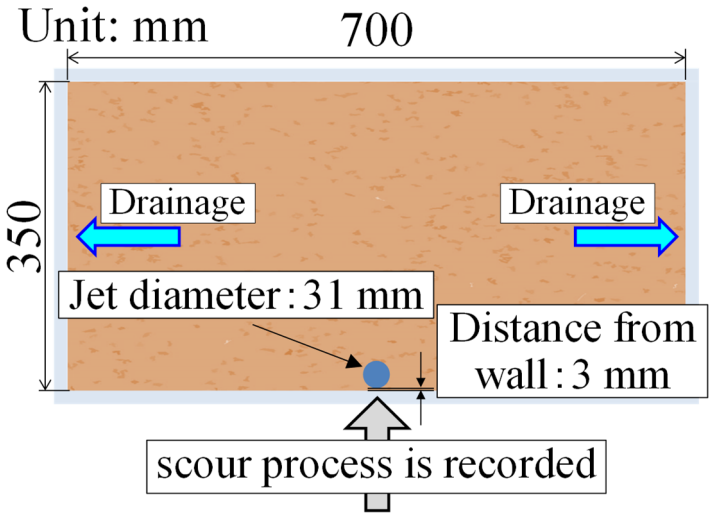

(b) Top view.

Fig. 1 Experimental apparatus.

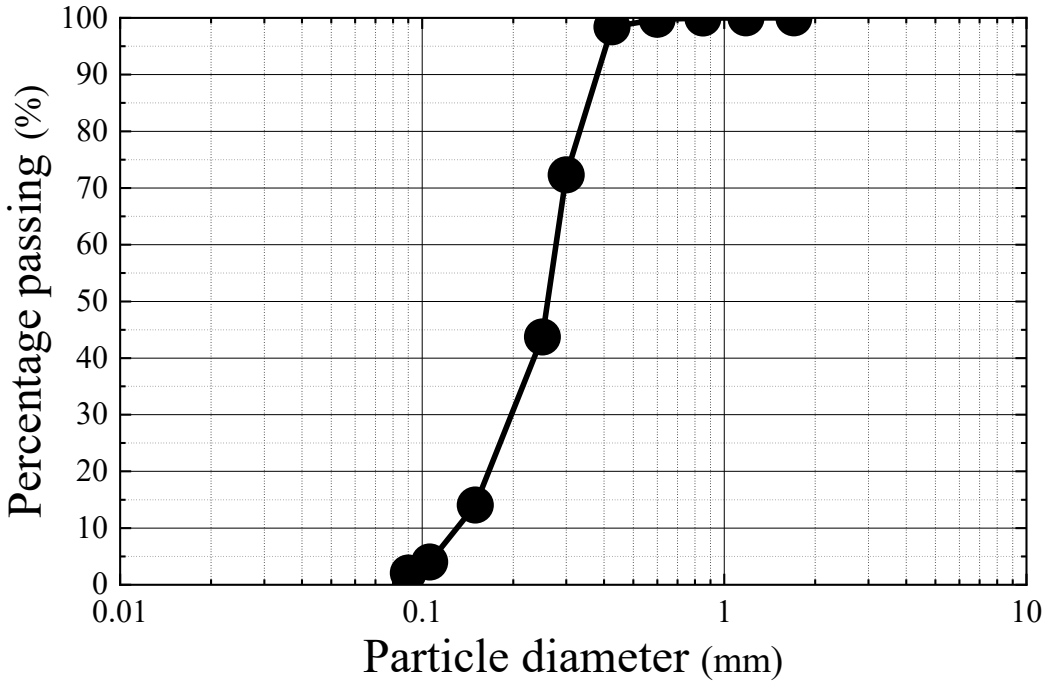

Fig.2 Size distribution of silica sand.

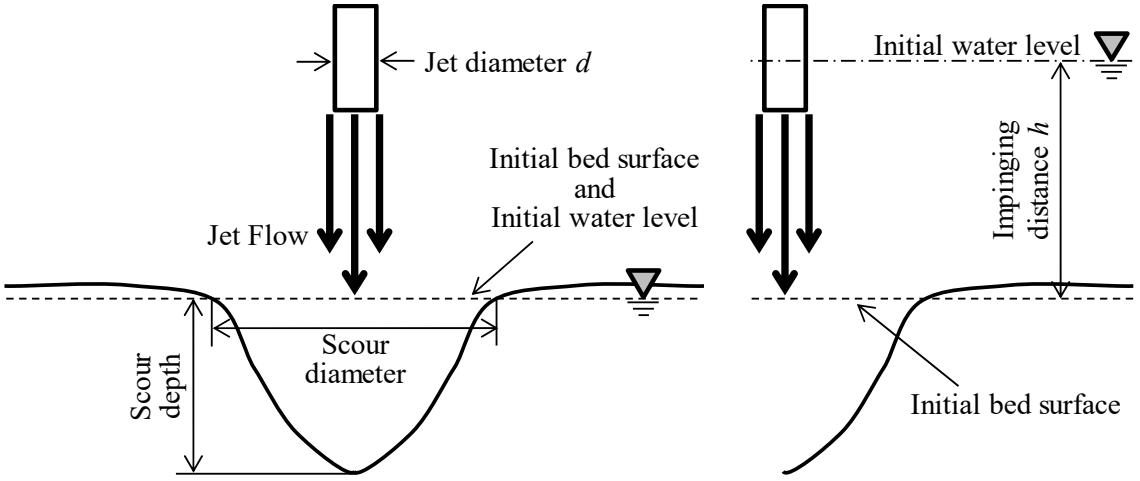

Fig. 3 Difference between the experimental conditions in the previous study and the present study. (Left: present study, Right: previous studies conducted by Rajaratnam 1981, Aderibigbe and Rajaratnam 1996, Yeh et al. 2009, Matsuda et al. 2014, and Matsuda et al. 2016).

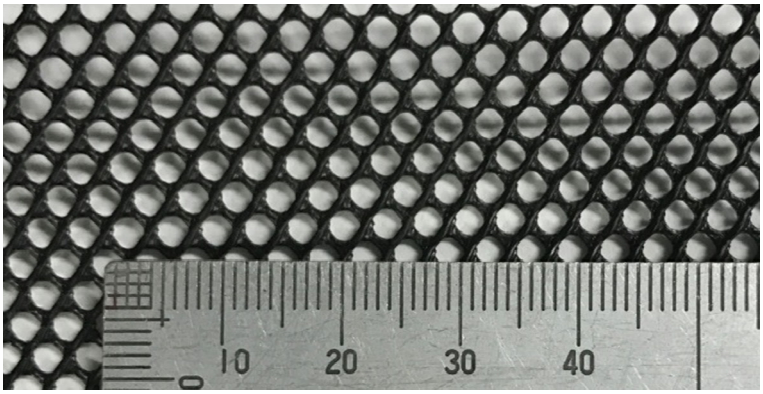

(a) Geonet (main raw material: polyethylene, mesh shape: circle, mesh size: 2.5 mm, and coverage ratio: 52.4%).

(b) Gravel (D_{50}: 15 mm).

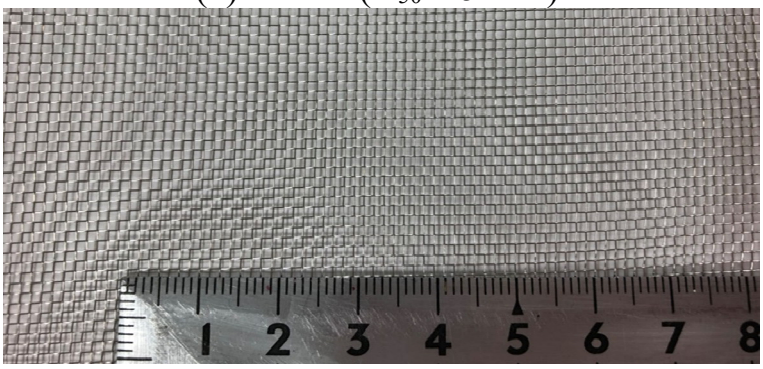

(c) Mesh sheet for Case 7 (main raw material: stainless steel, mesh shape: square, mesh size: 1.07 mm, and coverage ratio: 29.0%)

Fig. 4 Countermeasure work against scour used in the present experiments.

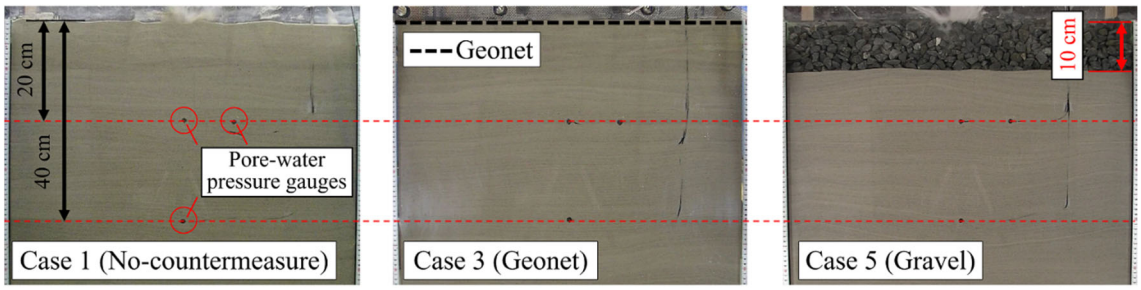

(a) 0 s

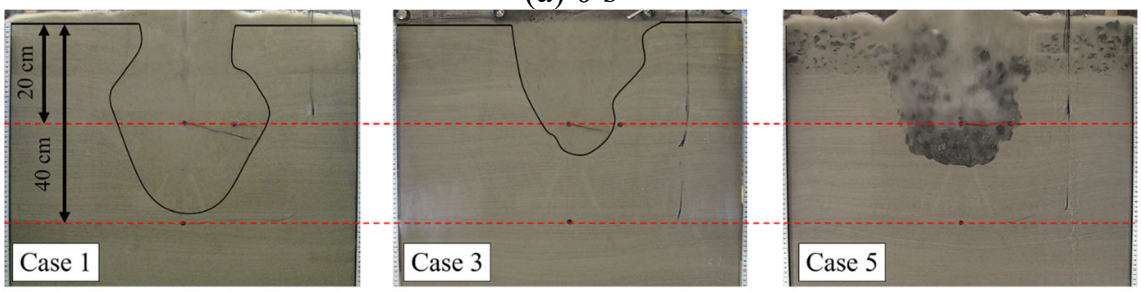

(b) 1 s

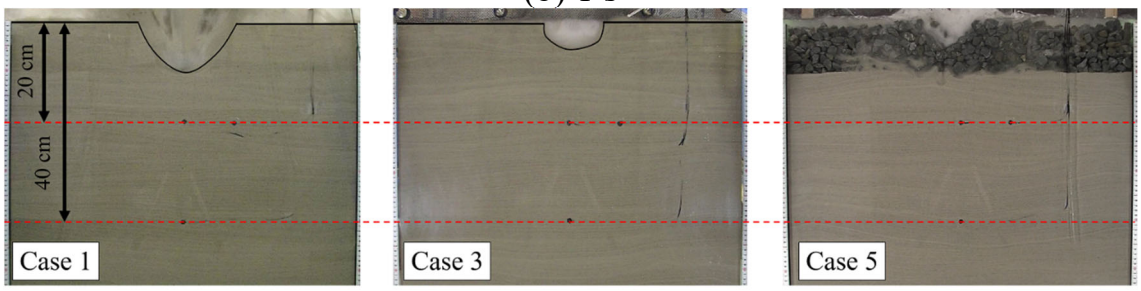

(c) 10 s

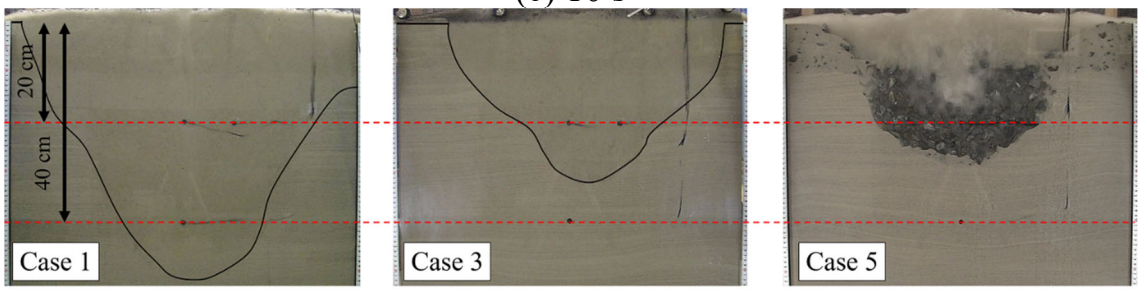

(d) 30 s

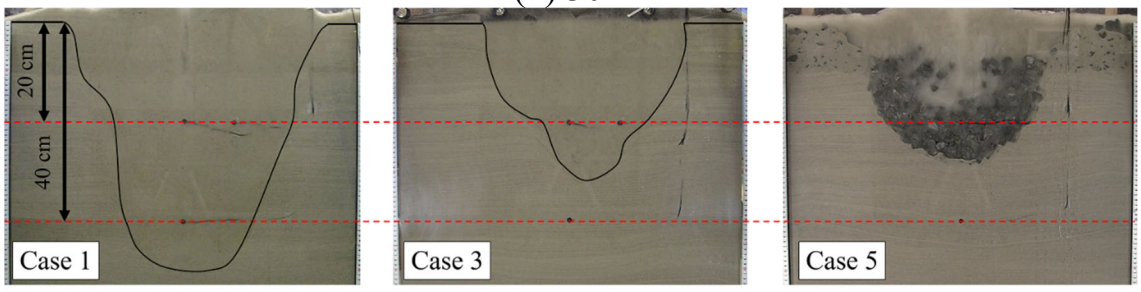

(e) 1 min

Fig. 5 Scour profiles at 1, 10, and 30 s and at 1 min (The sand bed surfaces for Case 1 and Case 3 are represented by a solid black line. The red dashed lines indicate the installation height of the pore-water pressure gauges).

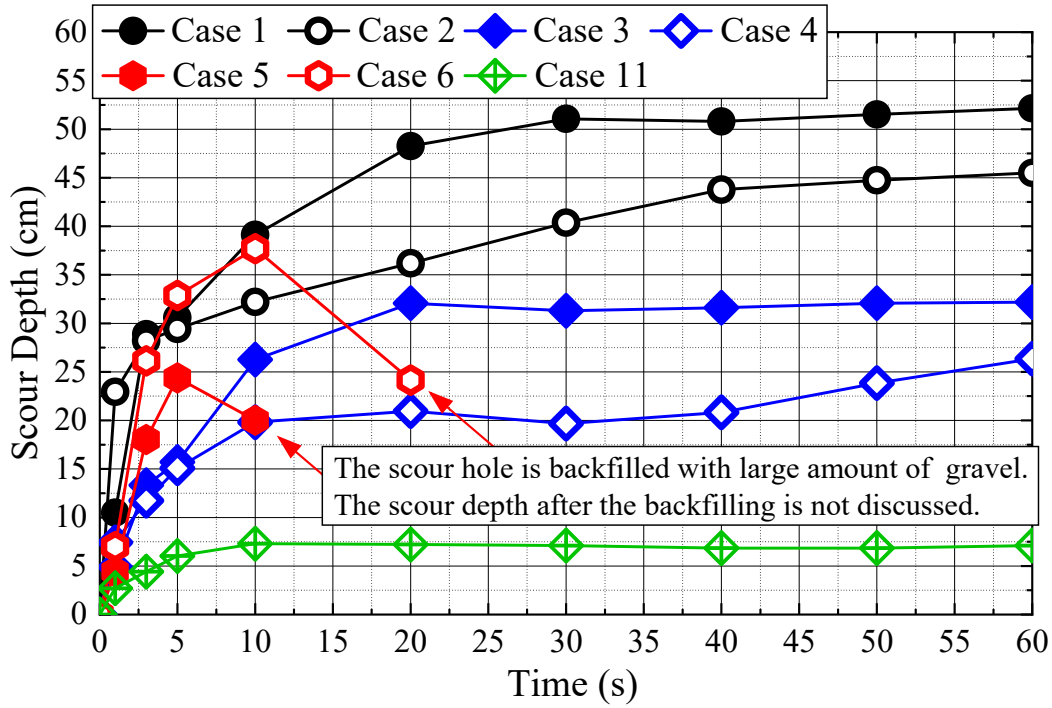

Fig. 6 Time variation of the scour depth for Cases 1–6.

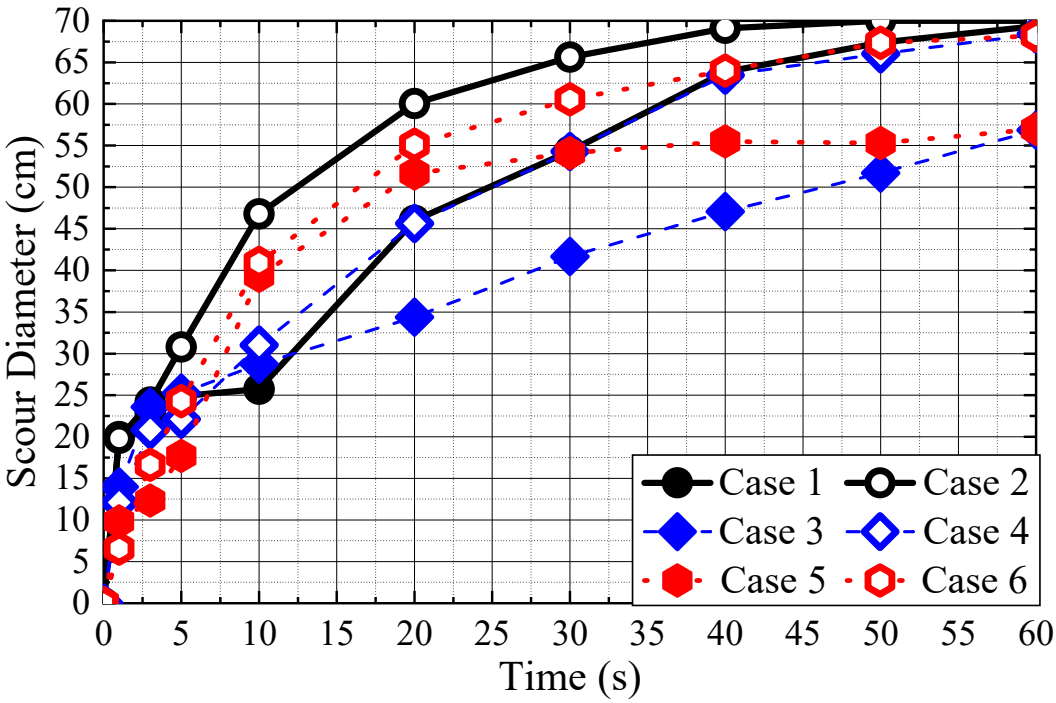

Fig. 7 Time variation of the scour diameter for Cases 1–6.

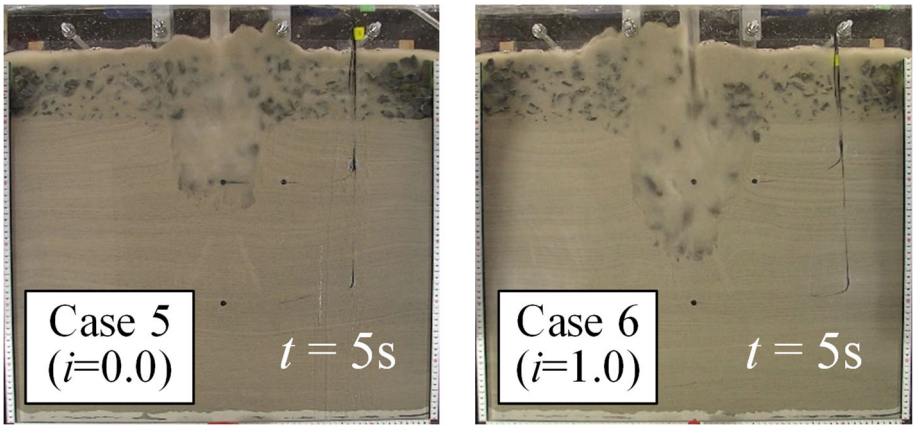

Fig. 8 Scour profile at 5 s with a scour countermeasure using gravel at each hydraulic gradient.

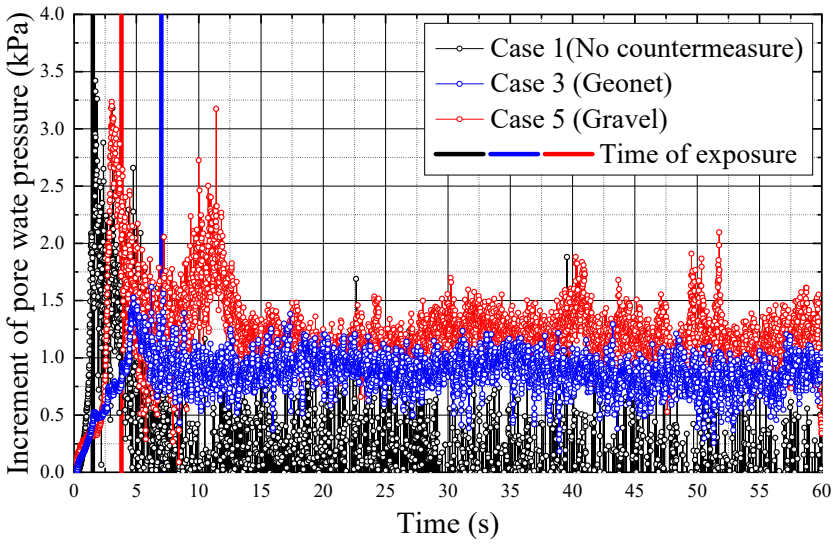

(a) Pore-water pressure gauge 1.

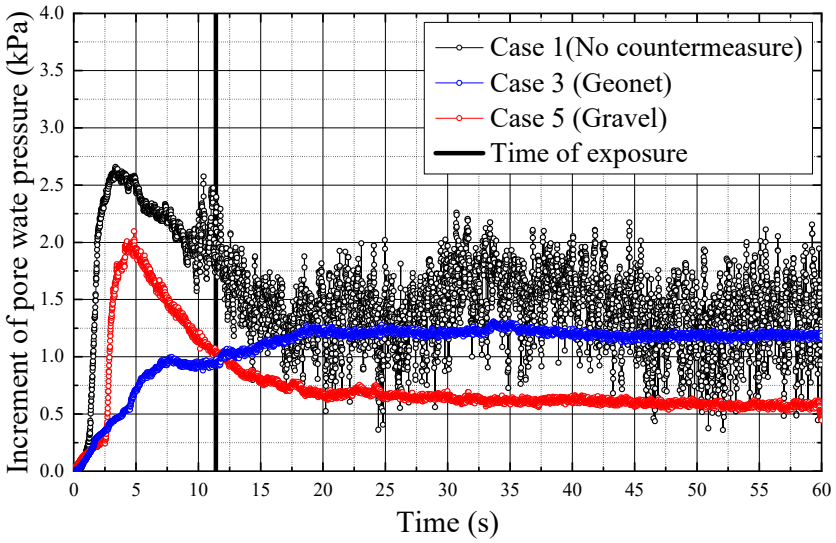

(b) Pore-water pressure gauge 2.

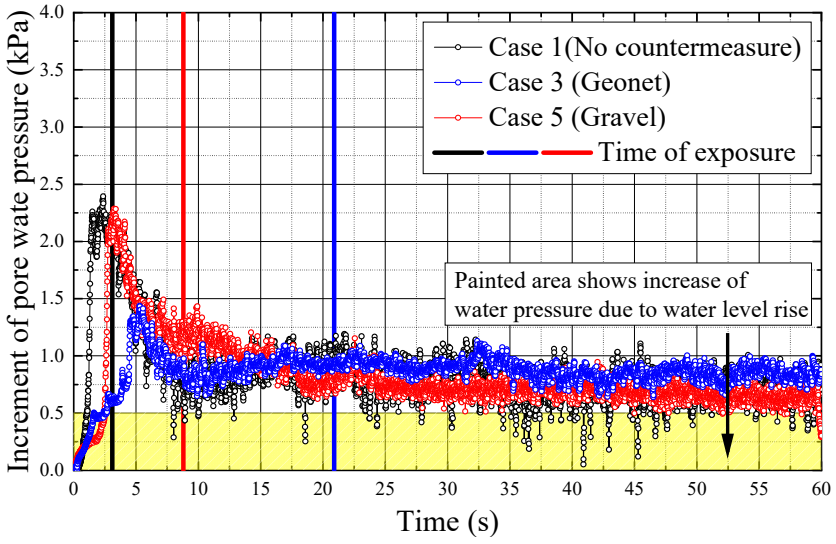

(c) Pore-water pressure gauge 3 (The painted area shows the increase in water pressure due to the water-level rise).

Fig. 9 Time variation of pore-water-pressure.

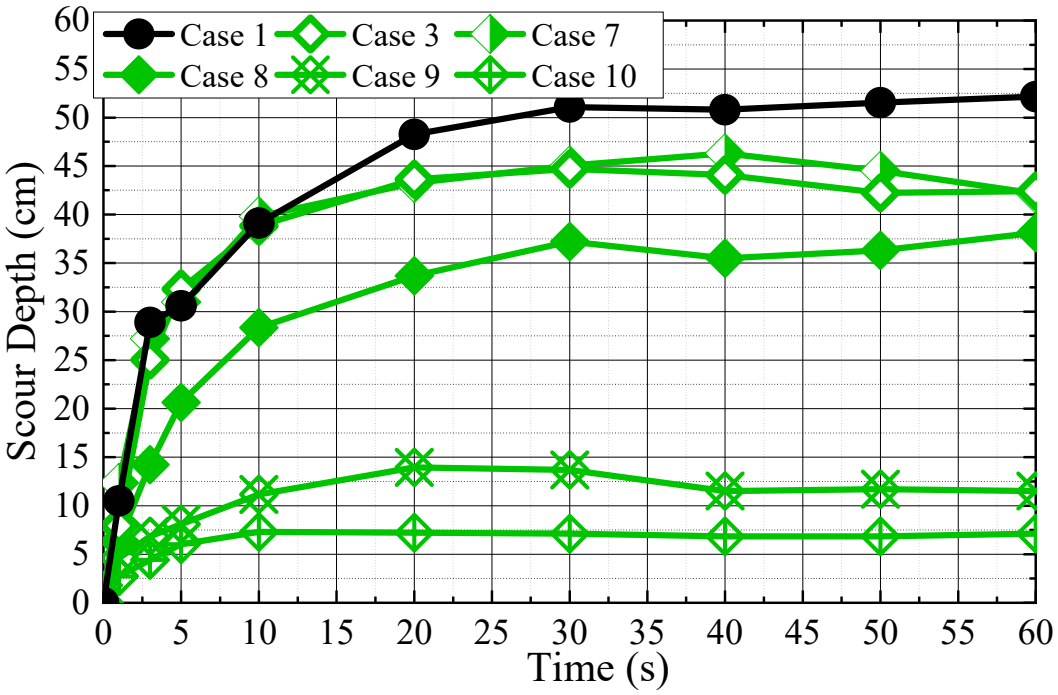

Fig. 10 Time variation of the scour depth for Cases 1 and 7–11.

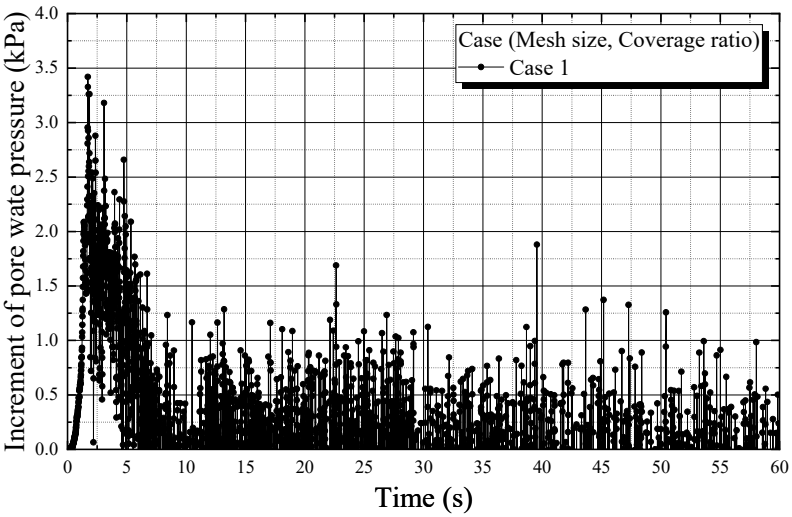

(a) Case 1.

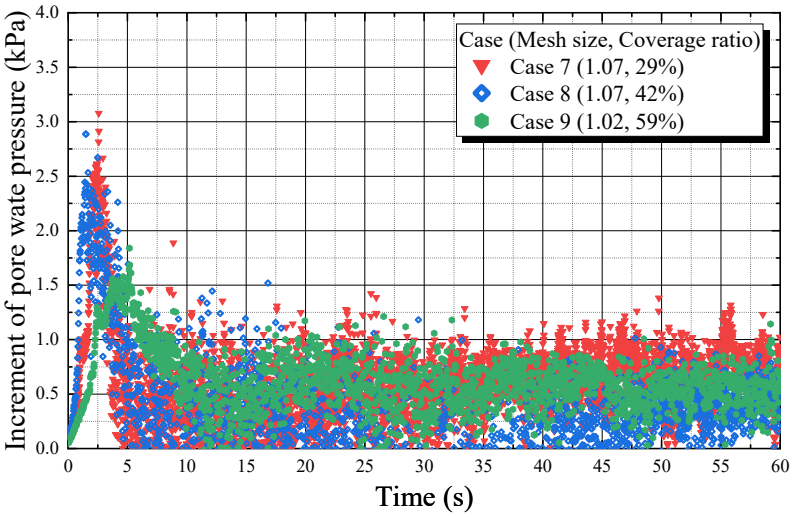

(b) Cases 7–9 (Mesh size: constant).

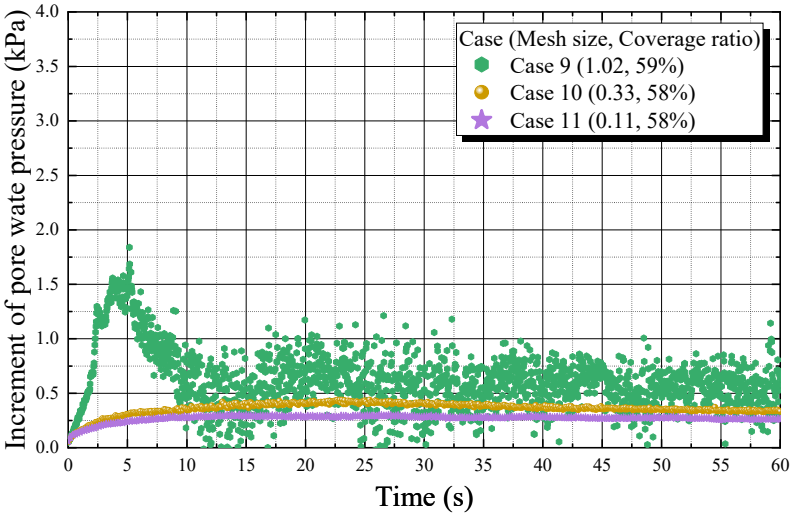

(c) Cases 9–11 (Coverage ratio: constant).

Fig. 11 Time variation of the pore-water pressure for Cases 1 and 7–11.

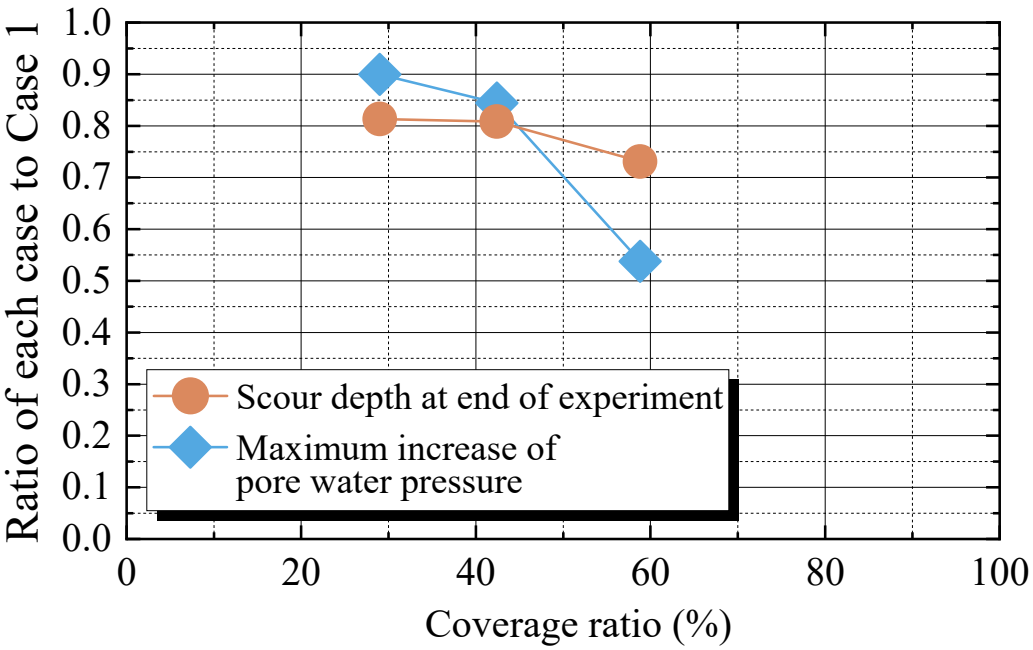

(a) Effect of the coverage ratio.

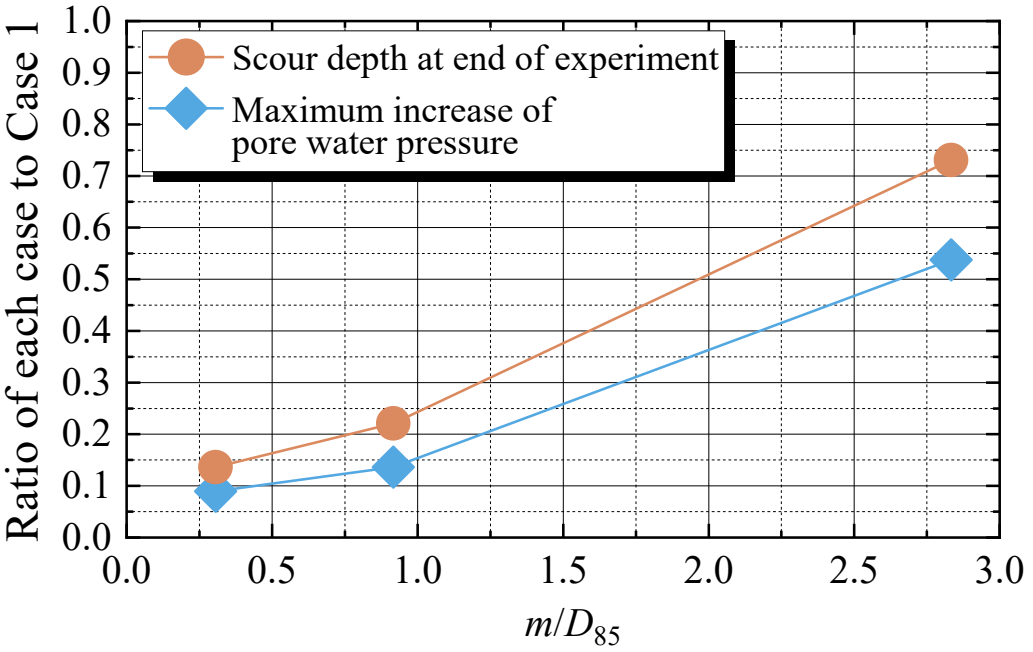

(b) Effect of the mesh size.

Fig. 12 Effect of coverage ratio and mesh size on the scour depth and pore-water pressure (The value measured at the pore-water-pressure gauge 1 is used).